Identification of an open crack in a beam using an a posteriori error estimator of the frequency response functions with noisy measurements

Béatrice Faverjon, Jean-Jacques Sinou

Identification of an open crack in a beam using an *a posteriori* error estimator of the frequency response functions with noisy measurements

B. Faverjon[1] and J-J. Sinou [2]

[1] LMT-Cachan UMR-CNRS 8535 (E.N.S. de Cachan / Université Paris 6 / CNRS), 61 avenue du Président Wilson, 94235 Cachan Cedex, France

[2] Laboratoire de Tribologie et Dynamique des Systèmes UMR-CNRS 5513, Equipe Dynamique des Structures et des Systèmes Ecole Centrale de Lyon, 36 avenue Guy de Collongue, 69134 Ecully Cedex, France.

Abstract

This paper presents a robust damage assessment technique for the nondestructive detection and size estimation of open cracks in beams. The damage detection, based on the constitutive relation error updating method, is used for the identification of the crack's location and size in a simply-supported beam. The transverse open crack is modeled through the introduction of the flexibility due to the presence of the crack, i.e. by reducing the second moment of area of the element at the crack's location.
This identification algorithm is illustrated through numerical examples involving different positions and sizes of a transverse open crack. We show that the detection of damage and the identification of the crack's size and position can be achieved with satisfactory precision, even if 20% noise has been added to the simulations and less than 5% of all displacements have been measured.

1 Introduction

The identification of the depth and position of cracks through nondestructive testing is important to ensure the integrity of structural components for a wide range of civil, mechanical and aeronautical engineering applications. Indeed, the importance of an early detection of cracks appears to be crucial for both safety and economic reasons and has led to the development of various methods.
The most useful damage localization methods based on vibration measurements are probably those based on changes in natural frequencies and mode shapes. Reviews of research works dealing with the problem of crack detection based on changes in modal parameters can be found in [1–4]. Indeed, it has been established that the presence of a crack drastically affects the dynamic behavior of structures. Depending on the crack's size and location, the stiffness of the structure is reduced and, therefore, so are its natural frequencies compared to the original crack-free structure. This shift in natural frequencies has been commonly used to investigate the crack's location and size. For example, some research works [5–7] have been devoted to the identification of a crack's size and location through the determination of the intersection point of the superimposed contours corresponding to the measured eigenfrequency variations due to the crack. This damage identification technique is

called the “frequency contour lines method”. In order to avoid the problem of a non-unique damage location in the case of a structural symmetric beam, Swamidas et al. [8] proposed to extend this crack identification method by adding an off-center mass to the simply-supported beam. Recently, Sinou [9] developed an extension of the frequency contour lines method based on the changes of frequency ratios in the cracked beam, thus avoiding the need for accurate knowledge of the material properties and frequencies of the crack-free beam. Moreover, Owolabi et al. [10] proposed a crack identification technique based not only on the measured changes in the first three natural frequencies (i.e. the frequency contour lines method), but also in the corresponding amplitudes of the measured acceleration frequency response functions. Using the frequency contours and amplitude contours of the first three modes, they demonstrated that the crack’s size and location can be determined uniquely. Recently, Dilena and Morassi [11, 12] proved that the measurement of an appropriate set of frequencies and antiresonance frequencies enables unique identification of damage. The theoretical results were confirmed by comparisons with numerical and experimental tests. The authors also suggested that the direction in which the nodal points move can point to the damage location [13]. In these works, the identification techniques were based on a shift in natural frequencies. Even though experimental validations of the damage identification methods based on frequency variations mentioned above have led to some interesting results, all these methods require precise measurements of the natural frequencies of the cracked system and, therefore, their accuracy is affected by the presence of noise in these measurements. Indeed, incorrect measurements of natural frequencies, vibration modes and forced vibration amplitudes may result in erroneous identification of the crack’s size and location. For example, Lele and Maiti [14] found errors in the crack’s location and depth of about 10%. Cerri and Vestroni [15] indicated that a small error in the data (a mean error of 0.5%) is usually amplified strongly and becomes more than 5% in identification of the damage parameters. Similarly, Sinou [16] recently showed that identification of the crack’s parameters for a simply-supported cracked beam using this type of damage identification technique can become very difficult if the noise level affecting the natural frequencies is greater than 4%.

Consequently, to develop a robust damage assessment technique for the nondestructive detection and size estimation of open cracks in beams, we propose to use model updating methods that minimize the discrepancy between the test data and the model by modifying the numerical model. A state-of-the-art review can be found in [17]. On the one hand, “direct methods” [18, 19] apply corrections to the model’s mass and stiffness matrices, but, unfortunately, do not take the physical meaning of these modifications into account. On the other hand, “indirect or parametric methods” update the model by changing its physical parameters. Three categories of cost functions can be considered: input residuals [20, 21], output residuals [22, 23], and the residual called “Constitutive Relation Error” (CRE). In this study, the CRE is used and provides a measure of the quality of the updated model which is essential for model validation. This approach has been shown to be effective in structural dynamics with updated mass, stiffness and damping matrices obtained through eigenmodes or forced vibrations [24–27]. The method is based on the Drucker error and can also take into account nonlinearities due to material behavior or to contacts. Let us also mention two similar approaches used in the case of free vibration problems: the Minimum Dynamic Residual Expansion (MDRE) method [28] and the Modeling Error in the Constitutive Equations (MECE) method [29, 30]. Finally, one should note that many other strategies for the resolution of crack identification problems have been proposed [31], such as the recent strategies based on the enclosure method or the virtual work principle, which enables the formulation of observation equations, with emphasis on the reciprocity gap concept.

In this paper, we propose to investigate the effectiveness and robustness of the CRE method in the identification of cracks of various depths and locations based on noisy measurements. The paper is organized as follows: first, we give a brief presentation of the modeling of an open transverse crack and the associated model of a simply-

supported cracked beam. Then, we introduce the damage identification technique based on the CRE updating method for the identification of the crack's location. Finally, we illustrate the effectiveness and robustness of the method through various numerical simulations corresponding to different physical configurations.

2 The modeling of a simply-supported beam with a transverse crack

2.1 Equations of motion

In this paper, we consider a beam with a circular cross section, 1m in length and 0.1m in diameter, divided into 30 Timoshenko beam finite elements with four degrees-of-freedom per node (see Figure 1). The beam is assumed to be simply supported at each end.
The equations of motion for the simply-supported cracked beam can be written as

$$[\mathbf{M}]\{\ddot{X}\} + [\mathbf{C}]\{\dot{X}\} + [\tilde{\mathbf{K}}]\{X\} = \{F_d(t)\} \tag{1}$$

where $\{X\}$ is the vector of the nodal DOFs of the system, t the instant of time, $[\mathbf{M}]$ the mass matrix, $[\tilde{\mathbf{K}}]$ the global stiffness matrix and $\{F_d(t)\}$ the external force vector, and where the dot represents the derivative with respect to time. $[\mathbf{C}]$ denotes the proportional damping matrix, which can be expressed as

$$[\mathbf{C}] = \alpha[\mathbf{M}] + \beta[\mathbf{K}] \tag{2}$$

where α and β are real constants.
$[\tilde{\mathbf{K}}]$ contains the stiffness reduction $[\mathbf{K}_{crack}]$ at the crack's location and is given by

$$[\tilde{\mathbf{K}}] = [\mathbf{K}] - [\mathbf{K}_{crack}] \tag{3}$$

where $[\mathbf{K}]$ is the stiffness matrix of the crack-free beam. The stiffness matrix $[\mathbf{K}_{crack}]$ of the cracked element will be given in the next section.
Finally, let us define the external force vector as

$$\{F_d(t)\} = \{F\}e^{i\omega t} \tag{4}$$

where ω is the forcing frequency and $\{F\}$ the amplitude vector.
The response vector can be written as $\{X(t)\} = \{X_0\}e^{i\omega t}$. Using Equation 1, the system governing the equation in the frequency domain is

$$\left(-\omega^2[\mathbf{M}] + i\omega[\mathbf{C}] + [\tilde{\mathbf{K}}]\right)\{X_0\} = \{F\} \tag{5}$$

We will perform the identification of the crack's size and location by considering the response simulated from Equation 5 to a given external force $\{F_d(t)\}$ and by using the CRE estimator described in the next section.

2.2 The cracked element

In order to represent the stiffness properties of the cracked cross section locally in an crack-free beam, the flexibility due to the presence of the transverse crack must be taken into account. For a comprehensive literature survey of various crack modeling techniques, see [32, 33].

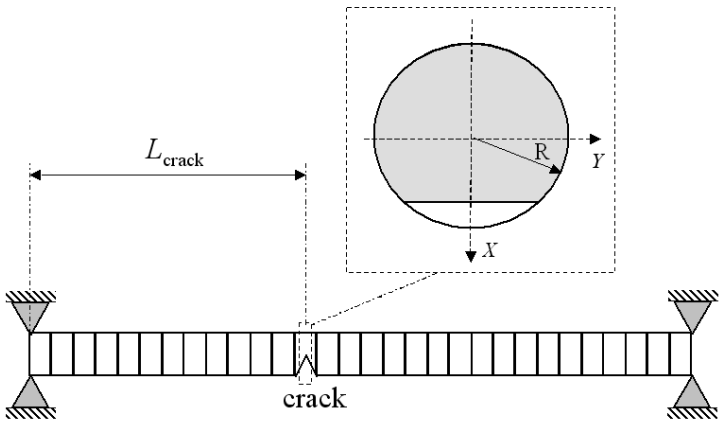

Figure 1: Finite-element model of the beam with the cracked cross section

In this study, the stiffness properties of the cracked cross section in a beam are represented locally using Mayes and Davies' transverse crack model [34, 35]. This model incorporates the flexibility due to the presence of the transverse crack by reducing the element's second moment of area at the location of the crack by ΔI. As explained by Mayes and Davies [36], the change in the m^{th} natural frequency of a system due to the presence of a transverse crack can be written as

$$\Delta\omega_m^2 = -g\left(\frac{d^2u_m}{dx^2}\right)_{x=s_c} \tag{6}$$

where u_m is the m^{th} mode shape of the beam and s_c the location of the crack along the beam. g is a function of the geometries of the crack and of the beam. Expanding on their analysis and using dimensional analysis to describe the stress concentration factor at the crack's front, they obtained the following expression [34]:

$$\Delta\omega_m^2 = -4\frac{EI^2}{\pi R^3}\left(1-\nu^2\right)F\left(\mu\right)\left(\frac{d^2u_m}{dx^2}\right)_{x=s_c} \tag{7}$$

where I, R, E and ν denote respectively the second moment of area, the shaft's radius and the material's Young's modulus and Poisson's ratio. $F\left(\mu\right)$ is a nonlinear compliance function which can be obtained from a series of experiments with chordal cracks [34, 35]. μ denotes the nondimensional crack depth and is given by

$$\mu = \frac{h}{R} \tag{8}$$

where h is the depth of the crack in the shaft as illustrated in Figure 2.
Then, using the second derivatives of the deflection curves, the bending moments M_0 and M of the original and cracked systems are given respectively by

$$M_0\left(s\right) = EI_0\left(s\right)\left(\frac{d^2y}{dx^2}\right)_{x=s} \tag{9}$$

and

$$M\left(s\right) = M_0\left(s\right) - \Delta M\left(s\right) = E\left(I_0\left(s\right) - \Delta I\left(s\right)\right)\left(\frac{d^2y}{dx^2}\right)_{x=s} \tag{10}$$

where y and s denote the deflection of the beam and the axial position. I_0 is the second moment of area of the original system.
In addition, assuming that the deflection curve is unchanged, the bending moments M_0 and M of the original and cracked systems are defined respectively by

$$M_0(s) = \omega_0^2 \int_0^s (s-z)\, m(z)\, y(z)\, dz \tag{11}$$

and

$$\Delta M(s) = \Delta\omega_0^2 \int_0^s (s-z)\, m(z)\, y(z)\, dz \tag{12}$$

where $m(z)$ corresponds to the mass per unit length at location z along the beam.
Using Equations 9-12 and Rayleigh's approach, Mayes and Davies [34] derived the relation:

$$\Delta\omega^2 = E\left(\frac{d^2y}{dx^2}\right)_{x=s}\left(\frac{\Delta I}{1-\frac{\Delta I}{I_0}}\right)\left(1-\frac{\Delta\omega^2}{\omega_0^2}\right) \tag{13}$$

By comparing Equations 7 and 13 and considering first-order changes in $\Delta\omega^2$ alone, Mayes and Davies obtained the following relation for a beam with a circular cross section:

$$\frac{\Delta I}{I_0} = \frac{\frac{R}{l}\left(1-\nu^2\right)F(\mu)}{1+\frac{R}{l}\left(1-\nu^2\right)F(\mu)} \tag{14}$$

where R and l are the shaft's radius and length respectively. Mayes and Davies [34, 35] proposed to obtain the evolution of $F(\mu)$ through a series of experiments with chordal cracks. This compliance function was later used by Sinou and Lees [37, 38] to study the dynamic behavior of a rotating shaft with a crack, taking into account the opening and closing of the crack at different orientations of the shaft due to its weight.
Then, using classical finite element formulation, the stiffness matrix $[\mathbf{K}_{crack}]$ at the crack's location modified by the transverse crack is:

$$[\mathbf{K}_{crack}] = \frac{E}{l^3}\begin{bmatrix} 12I_X & 0 & 0 & 6lI_X & -12I_X & 0 & 0 & 6lI_X \\ & 12I_Y & -6lI_Y & 0 & 0 & -12I_Y & -6lI_Y & 0 \\ & & 4l^2I_Y & 0 & 0 & 6lI_Y & 2l^2I_Y & 0 \\ & & & 4l^2I_X & -6lI_X & 0 & 0 & 2l^2I_X \\ & & & & 12I_X & 0 & 0 & -6lI_X \\ & & & & & 12I_Y & 6lI_Y & 0 \\ & & Sym. & & & & 4l^2I_Y & 0 \\ & & & & & & & 4l^2I_X \end{bmatrix} \tag{15}$$

The moments of inertia I_X and I_Y with respect to the parallel centroidal axes are given by [37]

$$I_X = \frac{R^4}{4}\left((1-\mu)\left(1-4\mu+2\mu^2\right)\gamma+\frac{\alpha}{2}\right) \tag{16}$$

and

$$I_Y = \frac{\pi R^4}{4} + R^4\left(\frac{2}{3}(1-\mu)\gamma^3+\frac{1}{4}(1-\mu)\left(1-4\mu+2\mu^2\right)\gamma+sin^{-1}(\gamma)\right)-\frac{4}{9}R^4\gamma^6\left((1-\mu)\gamma+\frac{\alpha}{2}\right)^{-1} \tag{17}$$

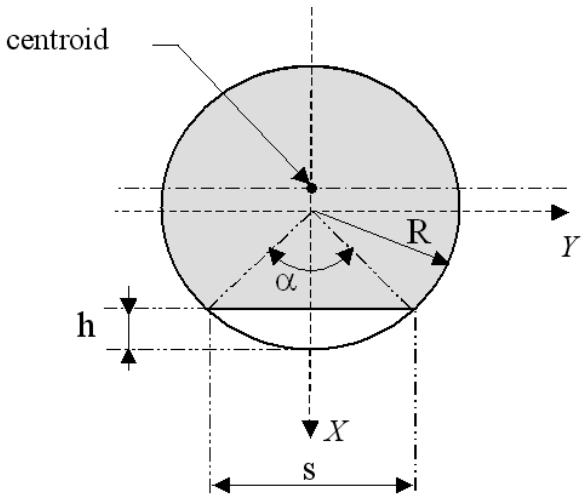

Figure 2: Cross section of the cracked beam

For convenience, $\gamma = \sqrt{2\mu - \mu^2}$. α is the crack's angle as shown in Figure 2 and is equal to $\alpha = 2cos^{-1}(1-\mu)$.

3 The constitutive relation error updating method

The Constitutive Relation Error (CRE) updating method, which uses an *a posteriori* estimator, has been widely and successfully used for validation problems in structural dynamics (see for instance [24–27]). It is presented in the next section in the general case. Its application to the simply-supported beam problem is described in Section 5.

3.1 The CRE estimator

We will only review the principles of the method. For further details, see [39].

Let Ω be the domain of the structure and $\partial\Omega$ its boundary (see Figure 3). The structure vibrates over a time interval $[0, T]$. Displacements $\underline{U}_d$ and forces $\underline{F}_d$ are prescribed respectively at boundaries $\partial\Omega_1$ and $\partial\Omega_2$, with $\partial\Omega_1 \cup \partial\Omega_2 = \partial\Omega$. Body forces $\underline{f}_d$ are applied within Domain Ω.

The reference problem consists in finding

$$s = (\underline{M}, t) = (\underline{U}(\underline{M}, t), \sigma(\underline{M}, t), \gamma(\underline{M}, t)) \qquad \underline{M} \in \Omega \quad , \quad t \in [0, T] \tag{18}$$

(respectively the displacement, the stress and the acceleration, $\underline{M}$ being the position vector) which verify a set of reliable equations and a set of less reliable equations. Here, since we are dealing with forced vibration problems, the equations will be expressed in the frequency domain. The reliable equations consist of the kinematic constraints and the equilibrium equations; the less reliable equations are the constitutive relations, which are written as

$$\sigma = \Big(\mathbf{K} + i\omega\mathbf{C}\Big)\epsilon(\underline{U}) \tag{19}$$

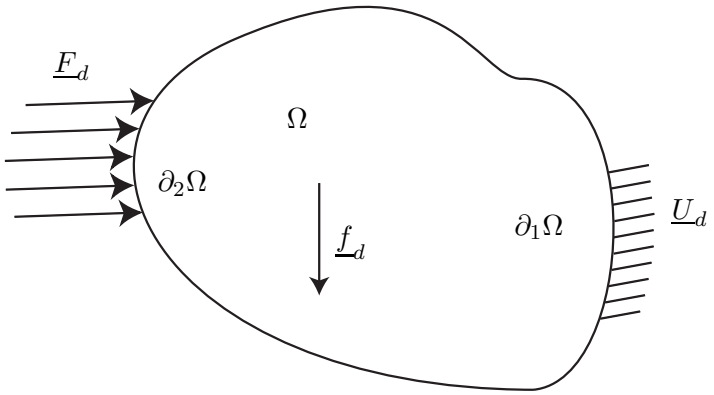

Figure 3: The domain being studied and the applied loads

$$\Gamma = -\rho\omega^2\underline{U} \tag{20}$$

where $\mathbf{K}$ is the Hooke's tensor (symmetric and positive definite), $\mathbf{C}$ the damping operator (symmetric, positive definite then ensuring the uniqueness of the solution and verifying Drucker's stability conditions, see [40]), ϵ the strain tensor and ρ the density. Drucker's stability conditions ensure the uniqueness of the solution and are verified by a large class of materials [39, 40]. We seek a solution which is admissible (i.e. which verifies the equations considered to be reliable). In the context of model updating, there are additional data which come from measurements. For a structure solicited at one point and whose displacements are measured at different locations, these quantities are also subdivided into a reliable set and a less reliable set. The reliable set consists of the measured angular frequency ω and the positions and directions of the excitations and sensors; the measured amplitudes of the forces $\underline{\widetilde{F}}_d$ and displacements $\underline{\widetilde{U}}_d$ at the excitation and sensor points are considered to be less reliable. Finally, the problem to be solved consists in finding admissible fields s which minimize the modified CRE e_ω^2 defined by

$$e_\omega^2 = \frac{\zeta_\omega^2}{D_\omega^2} + \frac{r}{1-r}\eta_\omega^2 \tag{21}$$

with a term corresponding to a modeling error:

$$\begin{aligned}\zeta_\omega^2(\underline{U},\underline{V},\underline{W}) = \int_\Omega \frac{\gamma}{2}\, tr[(\mathbf{K}+T\omega^2\mathbf{C})\,(\epsilon(\underline{V})-\epsilon(\underline{U})^\star(\epsilon(\underline{V})-\epsilon(\underline{U}))] \\ +\frac{1-\gamma}{2}\rho\omega^2(\underline{U}-\underline{W})^\star(\underline{U}-\underline{W})\,d\Omega\end{aligned} \tag{22}$$

a term corresponding to a measurement error:

$$\eta_\omega^2 = \frac{||\underline{U}|_{\partial_1\Omega} - \underline{\tilde{U}}_d||^2}{||\underline{\tilde{U}}_d||^2} + \frac{||\underline{F}|_{\partial_2\Omega} - \underline{\tilde{F}}_d||^2}{||\underline{\tilde{F}}_d||^2} \tag{23}$$

and displacements $\underline{U},\underline{V},\underline{W}$ which must verify

$$\underline{U}_c = \underline{U} \tag{24}$$

$$\sigma_s = \Big(\mathbf{K} + i\omega\mathbf{C}\Big)\epsilon(\underline{V}) \tag{25}$$

$$\underline{\Gamma}_s = -\rho\omega^2\,\underline{W} \tag{26}$$

where the static quantities σ and $\underline{\Gamma}$ are denoted σ_s and $\underline{\Gamma}_s$ and the dynamic quantity $\underline{U}$ is denoted $\underline{U}_c$. The symbol $\star$ designates the complex conjugate of a quantity. These equations are written for a given frequency ω. r is a weighting coefficient, which we will take equal to 0.5 [41], representing the degree of trust one has in the experimental data. The denominator D_ω^2 and the norms being used ensure that the two error terms have equivalent weights. The following expression can be used [41]:

$$D_\omega^2 = \int_\Omega \Big(\frac{\gamma}{2}\,tr[(\mathbf{K} + T\omega^2\mathbf{C})\,\epsilon(\underline{U})^\star\epsilon(\underline{U})] + \frac{1-\gamma}{2}\rho\omega^2\underline{U}^\star\underline{U}\Big)\,d\Omega \tag{27}$$

Finally, over the whole frequency range $[\omega_{min}, \omega_{max}]$, the modified error is calculated using a weighting factor $z(\omega)$ such that $\int_{\omega_{min}}^{\omega_{max}} z(\omega)d\omega = 1$ with $z(\omega) \geq 0$, e.g. $z(\omega) = 1/(\omega_{max} - \omega_{min})$. The error is given by

$$e_T^2 = \zeta_T^2 + \eta_T^2 \tag{28}$$

in which

$$\zeta_T^2 = \int_{\omega_{min}}^{\omega_{max}} \frac{\zeta_\omega^2}{D_\omega^2} z(\omega)d\omega \tag{29}$$

$$\eta_T^2 = \int_{\omega_{min}}^{\omega_{max}} \eta_\omega^2 z(\omega)d\omega \tag{30}$$

3.2 Implementation of the method

The updating of the parameters is carried out by minimizing the modified CRE. Such an inverse problem with no additional manipulation is ill-posed. Our updating method can be viewed as a regularization process leading to a unique solution of the problem. The method is iterative, each iteration consisting of two steps. The first step consists in localizing the most erroneous regions, then the most erroneous structural parameters; the second step consists in correcting the parameters belonging to these regions. The updating process is stopped when the threshold error is reached (for further details, see [26, 39, 40]).

In practice, the solution of the problem described in Section 3.1 enables one to calculate ζ_T^2 and e_T^2. The value of ζ_T^2 yields the relative quality (in $\%$) of the numerical model with respect to measurements over a frequency range, which is used to determine whether model updating is necessary. The first step of the model updating method consists in identifying which substructures have high model error values and can be achieved by calculating the model error of each substructure E and by choosing a level such as

$$\zeta_{ET}^2 \geq \tilde{\delta} \max_{E \in \mathbf{E}} \zeta_{ET}^2 \tag{31}$$

where $\mathbf{E}$ is the set of all the substructures and $\tilde{\delta}$ is a chosen value.

During the correction process, which is the second step of the model updating method, only the parameters from these substructures are updated. The final value of these parameters must correspond to a minimum of e_T^2. This problem, which is nonlinear with respect to these parameters, is solved using a BFGS minimization algorithm and the gradients of the parameters are calculated numerically. Besides, for each variation of the parameters, the mass, stiffness and damping matrices are reassembled. Once the correction has been made, the model error ζ_T^2 is recalculated. If the new value is less than a given level, the updating process is terminated; otherwise, a new iteration consisting of a localization step and a correction step is performed.

3.3 Discretization of the problem

The discrete form of the modified error is written with respect to the vectors (denoted $\{U\}$, $\{V\}$ and $\{W\}$) of the nodal values of the displacement fields $\underline{U}$, $\underline{V}$ and $\underline{W}$. In the case of a single excitation, the measured displacements are normalized by the amplitude of the force vector, so that only the amplitudes of the displacements appear in the expression of the error measure η_ω^2. Thus, Equation 23 depends on the displacements alone. Consequently, one has

$$e_\omega^2(\{U\},\{V\},\{W\}) = \frac{\gamma}{2}\{U-V\}^{T\star}([\mathbf{K}]+T\omega^2[\mathbf{C}])\{U-V\} + \frac{1-\gamma}{2}\omega^2\{U-W\}^{T\star}[\mathbf{M}]\{U-W\} + \frac{r}{1-r}\{\Pi U-\widetilde{U}\}^{T\star}[\mathbf{G}]\{\Pi U-\widetilde{U}\} \quad (32)$$

in which $\{U-V\}$ and $\{U-W\}$ denote $\{U\}-\{V\}$ and $\{U\}-\{W\}$ respectively. Moreover, Π is a projection operator which, when applied to a vector $\{Z\}$, yields the values of that vector at the sensors. The matrix $[\mathbf{G}]$ quantifies the error in the measurements. In our case, we used the following expression [42]:

$$[\mathbf{G}] = \frac{\gamma}{2}([\mathbf{k}]+T\omega^2[\mathbf{c}]) + \frac{1-\gamma}{2}\omega^2[\mathbf{m}] \quad (33)$$

where $[\mathbf{m}]$, $[\mathbf{k}]$ and $[\mathbf{c}]$ are respectively the reduced mass, stiffness and damping matrices of the system at the measurement points. In addition, the solution ($\{U\}$, $\{V\}$, $\{W\}$) must be admissible, i.e. it must verify

$$([\mathbf{K}]+i\omega[\mathbf{C}])\{V\} - \omega^2[\mathbf{M}]\{W\} = \{F\} \quad (34)$$

$\{F\}$ is the vector of the excitation forces. The minimization of the error e_ω^2 under the admissibility constraints is obtained by introducing Lagrange multipliers, which leads to the resolution of a system of linear equations given by

$$[\mathbf{A}]\{Y\} = \{B\} \quad (35)$$

where $[\mathbf{A}]$, $\{Y\}$ and $\{B\}$ are written as

$$[\mathbf{A}] = \begin{bmatrix} \frac{\gamma}{2}([\mathbf{K}]+T\omega^2[\mathbf{C}]) & \frac{1-\gamma}{2}\omega^2[\mathbf{M}] & \frac{r}{1-r}\Pi^T[\mathbf{G}]\Pi \\ \frac{\gamma}{2}([\mathbf{K}]+T\omega^2[\mathbf{C}]) & \frac{1-\gamma}{2}([\mathbf{K}]-i\omega[\mathbf{C}]) & \mathbf{0} \\ -[\mathbf{K}]-i\omega[\mathbf{C}] & \omega^2[\mathbf{M}] & [\mathbf{K}]+i\omega[\mathbf{C}]-\omega^2[\mathbf{M}] \end{bmatrix} \quad (36)$$

$$\{Y\} = \begin{bmatrix} \{U-V\} \\ \{U-W\} \\ \{U\} \end{bmatrix} \quad (37)$$

$$\{B\} = \begin{bmatrix} \frac{r}{1-r}\Pi^T[\mathbf{G}]\{\widetilde{U}\} \\ \mathbf{0} \\ \{F\} \end{bmatrix} \quad (38)$$

4 Calculation of the crack's depth

The CRE updating method described in the previous section enables one to identify the crack's position within a particular element of the shaft. Then, the calculation of the crack's depth may be carried out using the following strategy. Considering Equations 15, 16 and 17, the stiffness matrix $\mathbf{K}_{crack}$ modified by the transverse crack is expressed at the crack's location as a function of the nondimensional crack's depth $\mu = \frac{h}{R}$. Therefore, the identification of the crack's depth is achieved by minimizing the error e_μ^2 in the crack's depth with respect to the nondimensional crack depth μ:

$$e_\mu^2 = \sum_{i=1}^{8} \sum_{j=1}^{8} \left(\mathbf{K}_{crack,ij} - \mathbf{K}_{ident,ij}\right)^2 \tag{39}$$

where $\mathbf{K}_{crack,ij}$ and $\mathbf{K}_{ident,ij}$ denote the theoretical and identified flexibility coefficients respectively.

5 Numerical studies

In this section, in order to verify the suitability of the proposed approach, we will present eight numerical example cases with different damage locations and crack sizes. The position and size of the crack for each case is defined in Table 1.

These eight cases were chosen to demonstrate the robustness of the crack identification method with respect to the crack's depth and location. The crack sizes in the eight cases may be rearranged as follows:

- small crack depths: Cases 3, 6 and 7;
- intermediate crack depths: Cases 1 and 5;
- large crack depths: Cases 2, 4 and 8.

It is well-known that an eigenfrequency is unaffected if the crack is located at a node of the associated mode (i.e. at the center of the beam for the second vertical and horizontal modes, and at one-third or two-thirds of the beam for the third vertical and horizontal modes). In order to illustrate the robustness of the identification method when the crack is located near a node, Case 1 concerns a crack situated at a node of the third vertical and horizontal modes (at one-third of the beam) and Case 2 concerns a crack situated at the node of the second vertical and horizontal modes (at the center of the beam). Cases 4, 5, 6 and 7 concern a crack located near a node of the fourth vertical and horizontal modes. Finally, for Case 3, the crack is located near one end of the beam.

Moreover, since damage identification can be more or less difficult depending on the information available (e.g. the number, locations and directions of the sensors, or the presence of noise in the measurements), the robustness of the method was studied under all of these hypotheses. First of all, the effectiveness of the method was investigated for the eight cases by considering sensors all along the beam and in the two transverse directions, both without noise and with 5% noise. Then, damage identification was carried out for Cases 1 and 2 considering only five sensors along one direction and four noise levels (0%, 5%, 10% and 20%).

The objective of all these numerical examples was to demonstrate that damage detection and the identification of the crack's size and position can be obtained with adequate precision even if the crack is small and located near a node. Moreover, it should be noted that the highest noise level (20%) was added to the simulations and that less than 5% of the displacements were measured.

Case	Crack's location (element)	Nondimensional crack depth μ
1	10	0.5
2	15	0.7
3	28	0.3
4	7	1.0
5	7	0.5
6	7	0.2
7	7	0.1
8	5	0.8

Table 1: Specific data for Cases 1 to 8

For each study, we first calculated the experimental data corresponding to the forced response of the cracked beam to a solicitation. The beam considered in this section was described in Section 2. The geometrical and physical parameters of the beam, the frequency range and the properties of the solicitation applied to the beam are summarized in Table 2.

The discrepancy between the experiments and the data obtained from an initial model associated with a crack-free beam is high and can be observed by plotting the vertical and horizontal displacements of the crack-free and cracked beams for various crack depths and locations (see Figure 4). As explained by various researchers in the last few decades [37, 43–46], the presence of the crack reduces the stiffness of the structure and, therefore, the natural frequencies of the original crack-free beam. Basically, an increase in the nondimensional crack depth decreases the natural frequencies of the beam (see, for example, Cases 4 and 5 in Figure 4). The main changes in the natural frequencies occur in the vertical mode because of the beam's height and its influence on the crack, as indicated in Equation 16. The frequencies are unchanged when the crack is located at a node of the associated mode (for example, at the center of the beam for the second vertical and horizontal modes, see Case 2 in Figure 4), and the decrease in the natural frequencies is more pronounced when the crack is located at the antinodal points of the associated mode shape (for example, at the center of the beam for the first and third vertical and horizontal modes, and at one-third or two-thirds of the beam for the second vertical and horizontal modes; see the comparison between Case 2 and Cases 4-5 in Figure 4). Moreover, the presence of the crack induces changes not only in the natural frequencies, but also in the antiresonant frequencies [11]. Therefore, a change in natural frequencies and antiresonances is the common first step in the detection of a crack, as well as in the identification of both the crack's depth and its location.

In each study, the model error was rather high. Then, the localization step was performed and all local errors were calculated. The most erroneous element of the beam, corresponding to the highest local error, was determined. The updating process was carried out by varying only the parameter associated with this element. In the end, the errors were significantly reduced.

First, we considered Cases 1 to 8 with sensors located all along the beam and displacements measured in the two transverse directions. The measurements were assumed to be noise-free. Table 3 gives the modified and model errors for all these cases. Since the model error was rather high, we started with the localization step. Figure 5 shows the local errors along the length of the beam for the eight cases. One can see that since the most erroneous element corresponded to the location of the crack the localization step was successful in all cases. Following the updating process, the errors (given in Table 3) were relatively small.

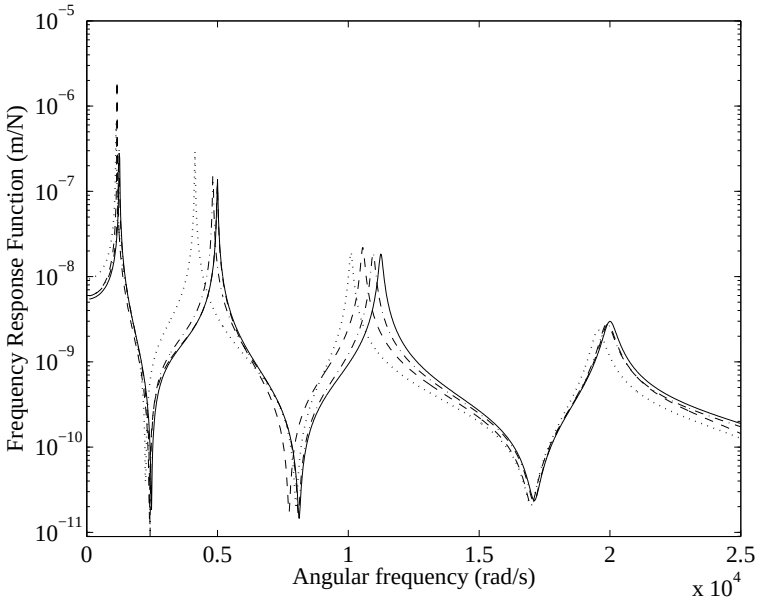

(a) Vertical direction

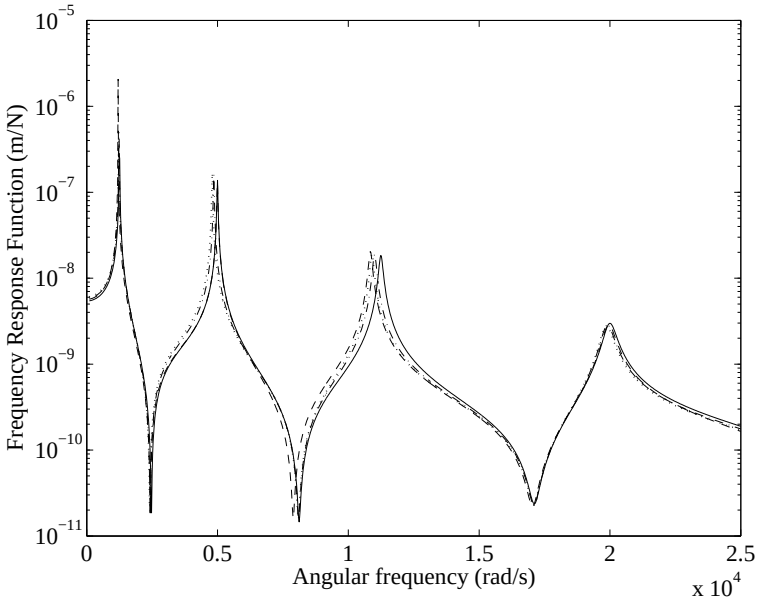

(b) Horizontal direction

Figure 4: Frequency response functions of the beam for various crack depths and locations at Element 5 of the beam (– crack-free, −− Case 2, ··· Case 4,–.– Case 5)

Young's modulus E (Pa)	2×10^{11}
Shear modulus G (Pa)	7.1×10^{10}
Density (kg/m^3)	7,800
Poisson's ratio ν	0.3
Radius of the cross section (m)	0.05
Length (m)	1
Damping coefficient α	0.66
Damping coefficient β	1.2×10^{-6}
Frequency range (rad/s)	$[100 \quad 25,000]$
Discretization of the frequency range (rad/s)	20
Location and directions of the excitation	Node 5, horizontal and vertical
Amplitude (N) of the excitation	$1/\sqrt{2}$

Table 2: Geometrical and physical parameters of the beam, frequency range of the study and nature of the excitation

Case	% noise	${\zeta_T^2}^i$	${e_T^2}^i$	${\zeta_T^2}^f$	${e_T^2}^f$
1	0	0.92	1.40	0.108	0.109
2	0	1.53	2.24	0.109	0.111
3	0	0.68	0.92	0.108	0.110
4	0	3.66	4.98	0.110	0.112
5	0	0.94	1.40	0.109	0.110
6	0	0.28	0.40	0.108	0.110
7	0	0.14	0.18	0.108	0.110
8	0	2.42	3.41	0.107	0.108

Table 3: Errors (in %) before (subscript i) and after (subscript f) the updating process for Cases 1 to 8 with no measurement noise

Then, the crack's size was obtained by minimizing the error in the crack's depth e_μ^2 (defined in Equation 39) with respect to the nondimensional crack depth ratio μ. The assumed and estimated nondimensional crack depths match perfectly in the eight cases, as shown in Table 4. At this stage of the study, one may point out that the crack model considered in this paper is a simplified model (with a regular cross section and a transverse crack with its front axis in the X-direction) which is generally accepted and used for the validation of model updating methods. Had the crack's shape at the cross section been different or the cross section irregular, the identification of the crack's size would have been erroneous. However, the crack's location would have been correctly identified because the crack modifies only the stiffness properties of the cracked cross section.

Since experimental data are usually affected by measurement noise, we studied the influence of various noise levels on the method. The random noise was distributed uniformly in space and over the frequency range. Table 5 shows the results for the eight previous cases, this time with 5% random measurement noise. Again,

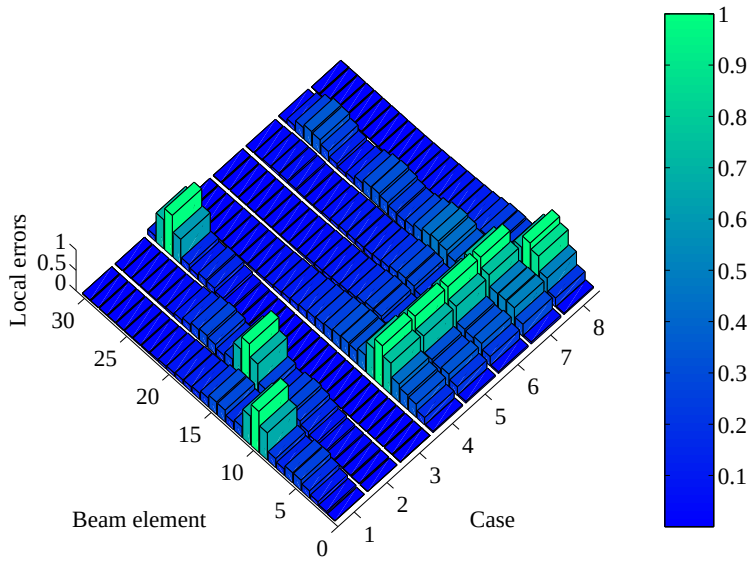

Figure 5: Local errors in the 30 elements (normalized to the highest value) for the eight cases with no measurement noise

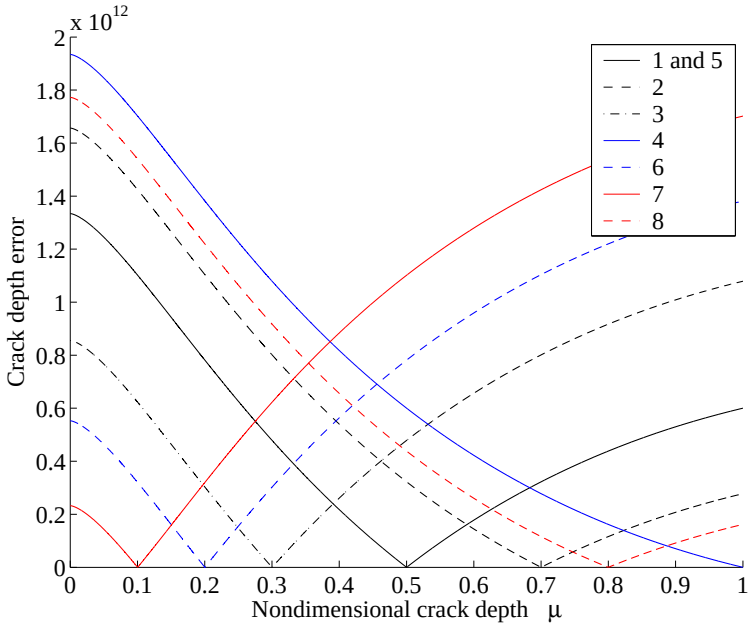

Figure 6: Error in the crack's depth for the eight cases with no measurement noise

Case	Assumed μ	Estimated μ (without noise)	Error (%) (without noise)	Estimated μ (with 5% noise)	Error (%) (with 5% noise)
1	0.5000	0.5001	0.02	0.5156	3.12
2	0.7000	0.7001	0.02	0.7059	3.12
3	0.3000	0.3002	0.02	0.2968	1.07
4	1.0000	1.0002	0.02	1.0200	2
5	0.5000	0.5002	0.04	0.5163	3.26
6	0.2000	0.2002	0.1	0.2267	13.35
7	0.1000	0.1003	0.3	0.1343	34.3
8	0.8000	0.8000	0	0.8087	1.09

Table 4: Comparison of assumed vs. identified nondimensional crack depth μ for Cases 1 to 8

Case	% noise	$\zeta_T^{2\,i}$	$e_T^{2\,i}$	$\zeta_T^{2\,f}$	$e_T^{2\,f}$
1	5	1.35	2.07	0.41	1.30
2	5	1.95	2.76	0.42	1.31
3	5	0.83	1.60	0.43	1.31
4	5	5.32	6.18	0.41	1.31
5	5	1.45	2.11	0.41	1.31
6	5	0.62	1.41	0.41	1.31
7	5	0.48	1.33	0.42	1.31
8	5	3.39	4.17	0.40	1.31

Table 5: Errors (in %) before (subscript i) and after (subscript f) the updating process for Cases 1 to 8 with measurement noise

for each case, the model error was rather large and yet the localization step was successful (see Figure 7). The errors following the updating process are given in Table 5. One can observe that the model error increases with the nondimensional crack depth ratio μ as well as with the level of measurement noise.

The nondimensional crack depth estimated from the crack depth error function defined in Equation 39 correctly matched the assumed nondimensional crack depth in all eight cases as shown in Table 4. However, one can observe that noise in the measurements can make the identification of the size of small cracks more difficult (see Cases 6 and 7 in Table 4).

Usually, measurements can be performed only at a few sensors, in one direction, and are unfortunately very noisy. In order to show the robustness of the method, we chose to calculate Cases 1 and 2 with only five sensors (located at Nodes 6, 11, 16, 21 and 26), in one direction and with various levels of measurement noise. The noiseless case was also considered so results with and without noise could be easily compared. Table 6 shows the results obtained after one localization step followed by the updating process. Figures 8(a) and 9(a) illustrate the local errors in the 30 elements (normalized to the highest value). In all cases, the final identification of the crack's location appears to be in agreement with the assumed position of the crack.

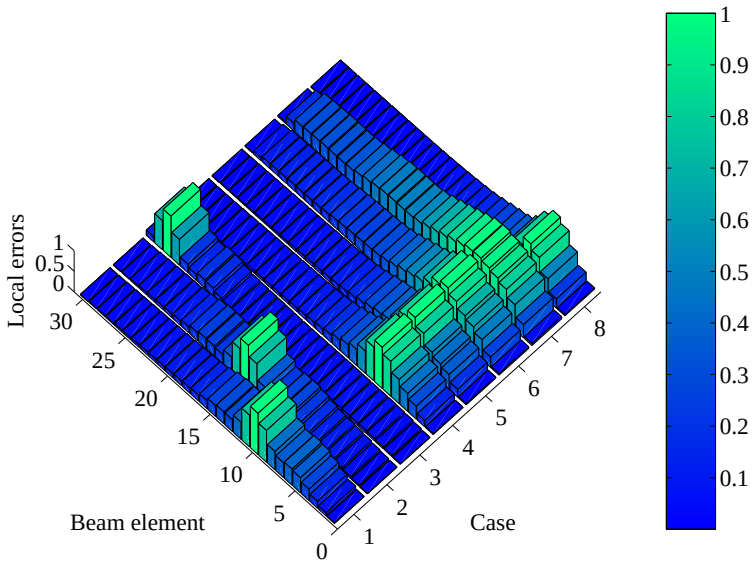

Figure 7: Local errors in the 30 elements (normalized to the largest value) for the eight cases with 5% random measurement noise

Then, the determination of the nondimensional crack depth was obtained by minimizing the crack depth error function. The results are given in Table 7. Figures 8(b) and 9(b) illustrate the evolutions of the error in the crack's depth. Even though the difference between the estimated and assumed nondimensional crack depths increases with the noise level, these results can be considered to be reasonably good. This proves that with 10% and 20% noise the crack's location obtained is perfect and the maximum errors in the estimation of the crack's size are about 7% and 13% respectively.

Finally, the comparisons of the Frequency Response Functions (FRFs) in the vertical direction obtained using the estimated crack parameters (i.e. the crack's location and nondimensional depth after minimization, indicated with red dotted-dashed lines) with the measurements generated from the assumed theoretical crack locations and depths (black solid line) are shown in Figures 10 to 13 and 14 to 17 for Case 1 and Case 2 respectively. For each case, the four figures correspond to calculations with four random noise levels (0%, 5%, 10% and 20%) affecting the assumed FRFs. Perfect agreement between the estimated and assumed vertical FRFs is clearly observed in most of the frequency range. The crack-free vertical FRF (black dashed lines) is shown to indicate the initial configuration used for the CRE updating method. It appears clearly that the estimated vertical amplitudes are very close to their actual values, even though 20% noise was added to the numerical simulations and less than 5% of the displacements were measured.

6 Conclusion

This research deals with the nondestructive detection of cracks in a simply-supported beam. The cracked beam is modeled by taking into account the flexibility due to the presence of the open transverse crack and by reducing the second moment of area of the element at the crack's location.

case	noise (%)	$\zeta_T^{2\,i}$	$e_T^{2\,i}$	$\zeta_T^{2\,f}$	$e_T^{2\,f}$
1	0	0.86	1.07	0.075	0.076
1	5	0.96	1.25	0.30	0.53
1	10	1.13	1.58	0.58	1.04
1	20	1.56	2.38	1.11	1.98
2	0	1.63	1.96	0.076	0.077
2	5	1.71	2.08	0.30	0.53
2	10	1.83	2.31	0.58	1.03
2	20	2.17	2.94	1.12	1.98

Table 6: Errors (in %) before (subscript i) and after (subscript f) the updating process for cases 1 and 2 with sensors in 5 displacements and with various levels of noise

case	noise (%)	Assumed μ	Estimated μ	Error (%)
1	0	0.5000	0.5001	0.02
1	5	0.5000	0.5164	3.28
1	10	0.5000	0.5340	6.8
1	20	0.5000	0.5662	13.24
2	0	0.7000	0.7001	0.01
2	5	0.7000	0.7084	1.2
2	10	0.7000	0.7170	2.43
2	20	0.7000	0.7343	4.9

Table 7: Comparison of the assumed and identified non-dimensional crack depth μ for cases 1 and 2 with sensors in 5 displacements and with various levels of noise

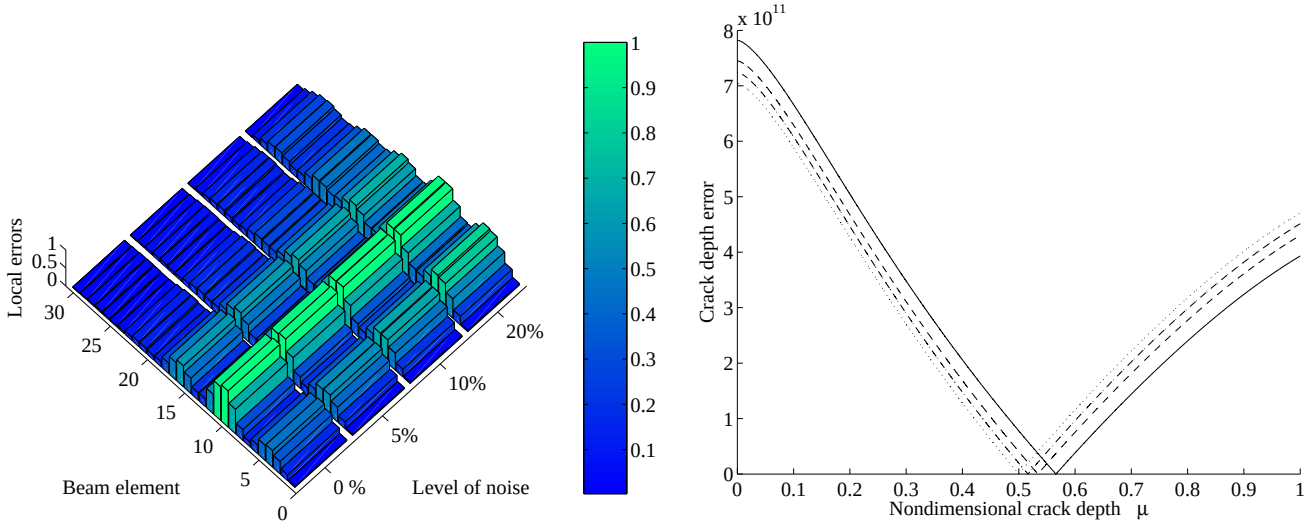

(a) Local errors

(b) Crack depth error with noise
($\cdots$ 0%, $--$ 5%, $-.-$ 10%, $-$ 20%)

Figure 8: Local errors in the 30 elements (normalized to the highest value) and evolution of the error in the crack's depth for Case 1 with noisy measurements and only with five sensors in one direction

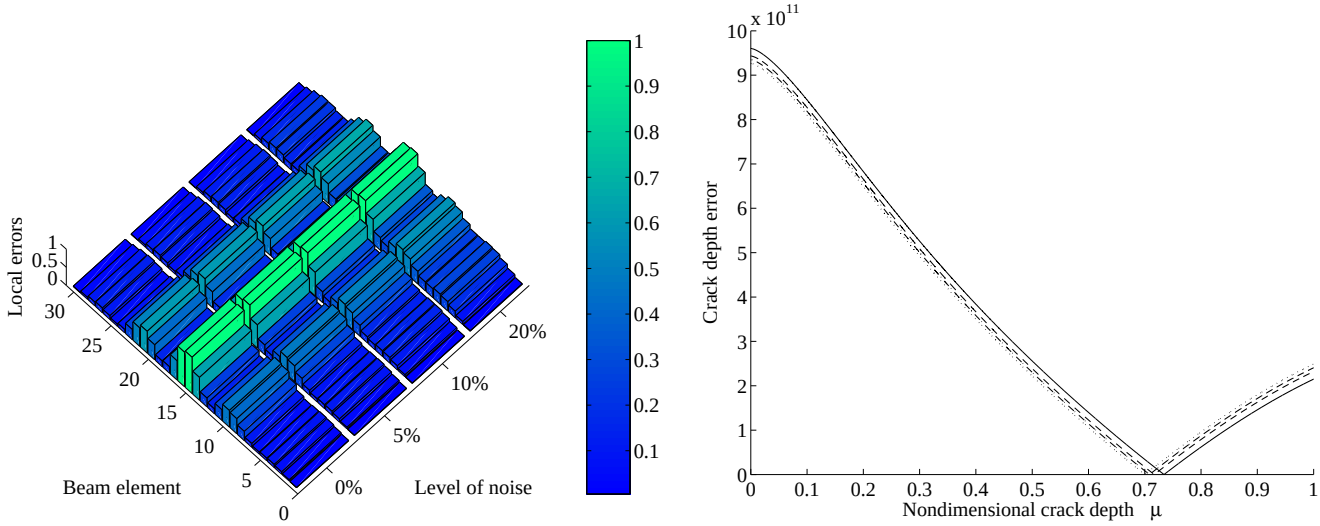

(a) Local errors

(b) Crack depth error with noise
($\cdots$ 0%, $--$ 5%, $-.-$ 10%, $-$ 20%)

Figure 9: Local errors in the 30 elements (normalized to the highest value) and evolution of the error in the crack's depth for Case 2 with noisy measurements and only with five sensors in one direction

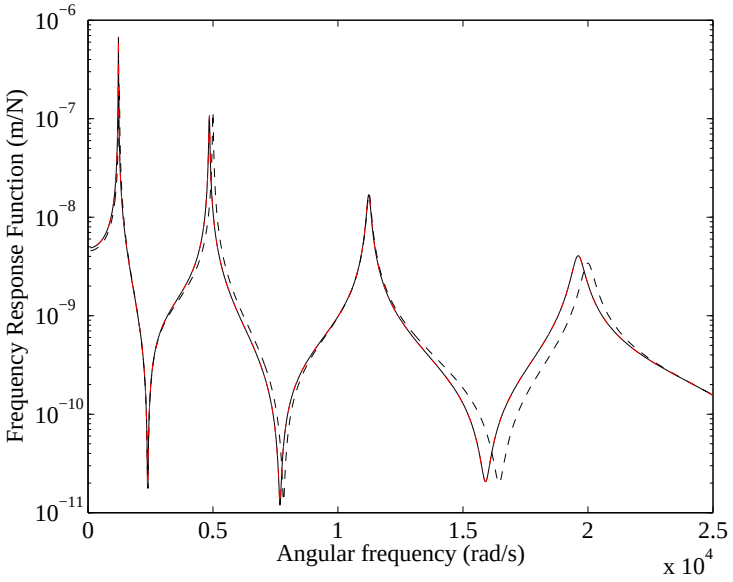

Figure 10: Comparison of the frequency response functions (vertical direction) for the cracked model (solid line), the reference healthy model (dashed lines) and the updated model (red dotted-dashed lines), obtained at Element 5 for Case 1 without noise

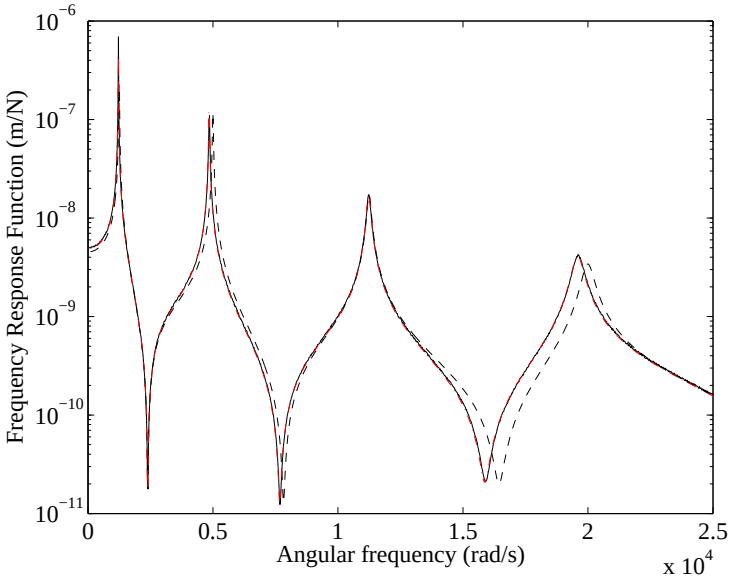

Figure 11: Comparison of the frequency response functions (vertical direction) for the cracked model (solid line), the reference healthy model (dashed lines) and the updated model (red dotted-dashed lines), obtained at Element 5 for Case 1 with 5% random noise

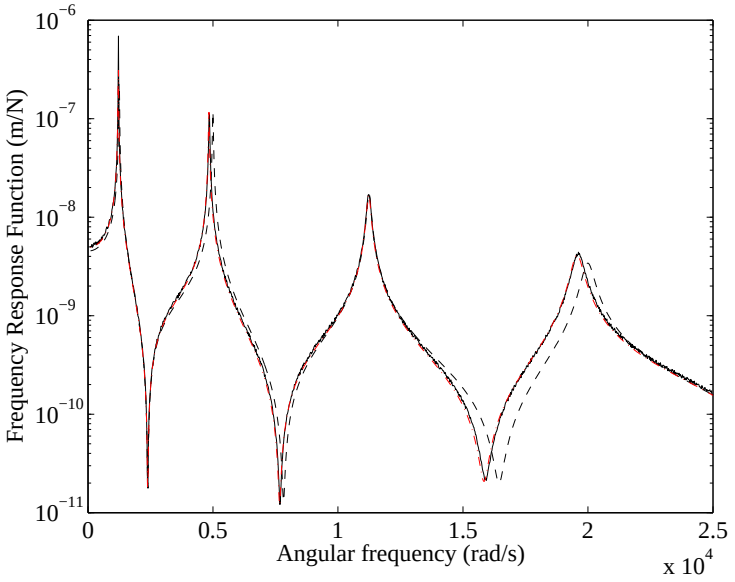

Figure 12: Comparison of the frequency response functions (vertical direction) for the cracked model (solid line), the reference healthy model (dashed lines) and the updated model (red dotted-dashed lines), obtained at Element 5 for Case 1 with 10% random noise

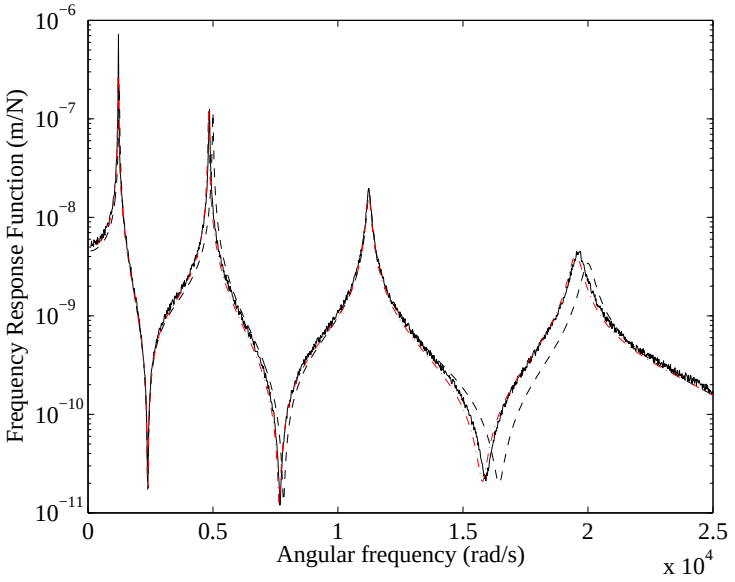

Figure 13: Comparison of the frequency response functions (vertical direction) for the cracked model (solid line), the reference healthy model (dashed lines) and the updated model (red dotted-dashed lines), obtained at Element 5 for Case 1 with 20% random noise

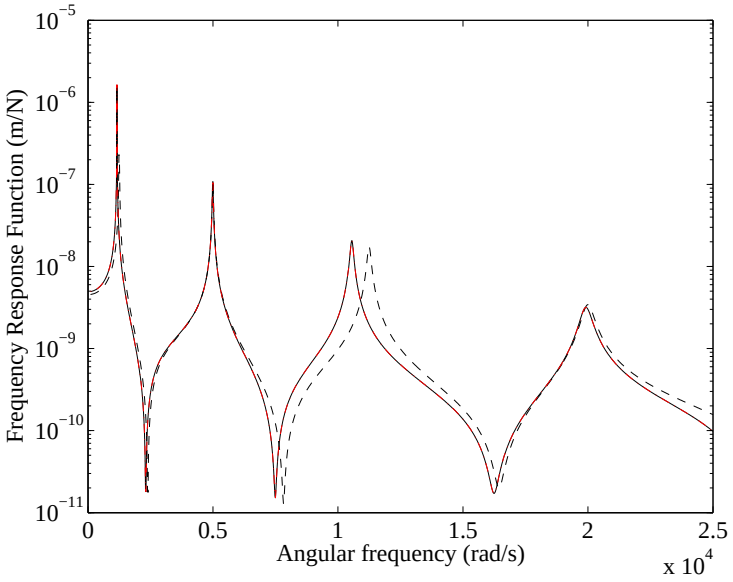

Figure 14: omparison of the frequency response functions (vertical direction) for the cracked model (solid line), the reference healthy model (dashed lines) and the updated model (red dotted-dashed lines), obtained at Element 5 for Case 2 without noise

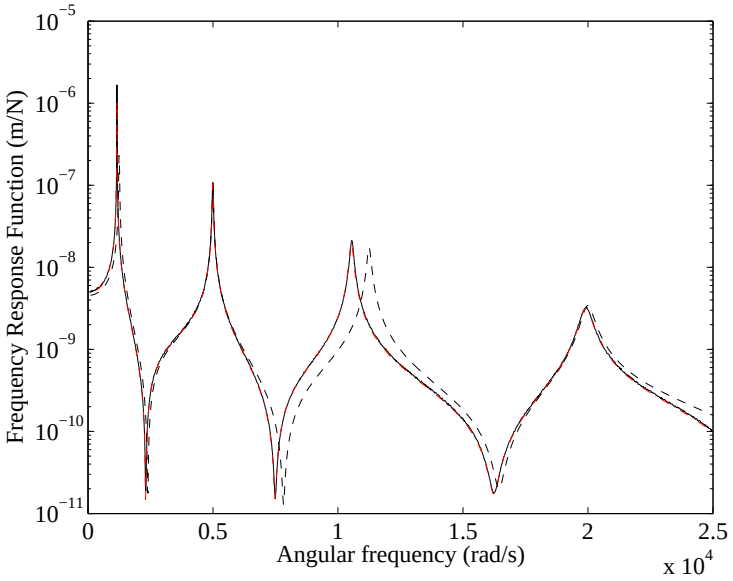

Figure 15: Comparison of the frequency response functions (vertical direction) for the cracked model (solid line), the reference healthy model (dashed lines) and the updated model (red dotted-dashed lines), obtained at Element 5 for Case 2 with 5% random noise

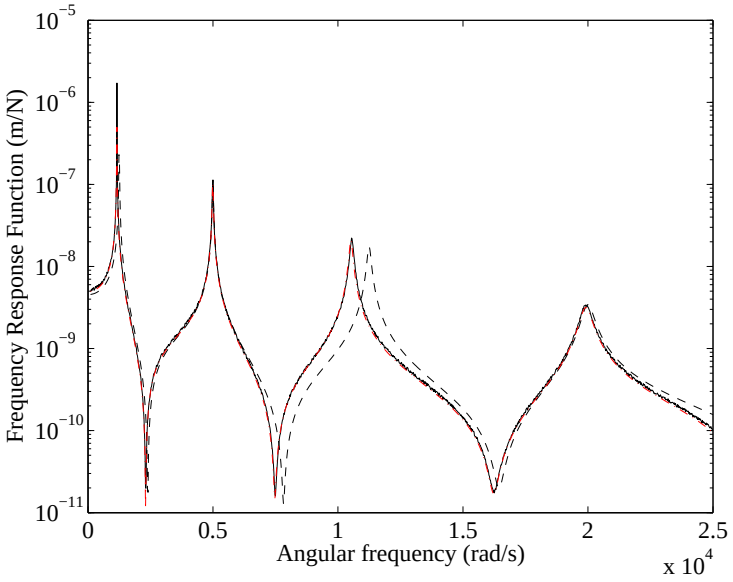

Figure 16: Comparison of the frequency response functions (vertical direction) for the cracked model (solid line), the reference healthy model (dashed lines) and the updated model (red dotted-dashed lines), obtained at Element 5 for Case 2 with 10% random noise

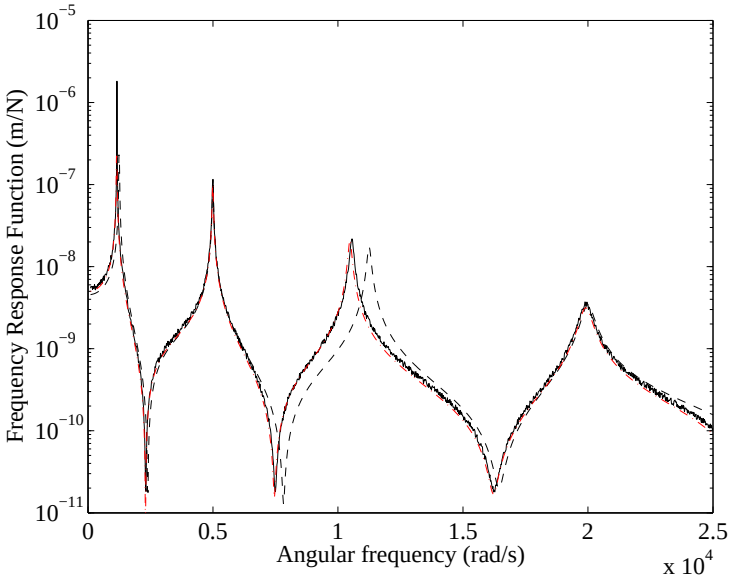

Figure 17: Comparison of the frequency response functions (vertical direction) for the cracked model (solid line), the reference healthy model (dashed lines) and the updated model (red dotted-dashed lines), obtained at Element 5 for Case 2 with 20% random noise

The damage assessment technique, based on the CRE updating method and a crack depth error function, was developed in order to identify the crack's location and its nondimensional size. The effectiveness of the proposed method is demonstrated through numerical simulations involving different crack locations and nondimensional crack depths. These examples show that the identification of the crack's parameters can be carried out with satisfactory precision even when the crack is located near a node of a vertical or horizontal mode or when the nondimensional crack depth is small. Moreover, these results demonstrate the robustness of the technique when 20% uniformly distributed noise is added to the simulations and less than 5% of the displacements are measured.

The results obtained with this robust damage detection tool combining a model error estimator and model updating procedure (proposed by Ladeveze and co-workers [24–27]), and the use of antiresonant frequencies (proposed by Dilena and Morassi [11]) are encouraging. The procedure for determining the crack's location and depth appears to be both simple and general. Future works will focus on assessing the effectiveness and limitations of the method based on more complex illustrative examples (3D structures with beam networks).

References

[1] Montalvao, D., Maia, N., and Ribeiro, A., 2006. "A review of vibration-based structural health monitoring with special emphasis on composite materials". *The Shock and Vibration Digest,* **38(4)**, pp. 1–30.

[2] Doebling, S., Farrar, C., Prime, M., and Shevitz, D., 1996. *Damage Identification and Health Monitoring of Structural and Mechanical Systems from Changes in Their Vibration Characteristics: A Literature Review*. Technical Report LA-13070-MS, Los Alamos National Laboratory Report.

[3] Sohn, H., Farrar, C., Hemez, F., Shunk, D., Stinemates, D., and Nadler, B., 2003. *A Review of Structural Health Monitoring Literature : 1996-2001*. Technical Report LA-13976-MS, Los Alamos National Laboratory Report.

[4] Salawu, O. S., 1997. "Detection of structural damage through changes in frequency: a review". *Engineering Structures,* **19(9)**, pp. 718–723.

[5] Dong, G., Chen, J., and Zou, J., 2004. "Parameter identification of a rotor with an open crack". *European Journal of Mechanics A/Solids,* **23**, p. 325–333.

[6] Nikolakopoulos, P., Katsareas, D., and Papadopoulos, C., 1991. "Crack identification in frame structures". *Computers and Structures,* **64(14)**, pp. 389–406 .

[7] Li, B., Chen, X., Ma, J., and He, Z., 2005. "Detection of crack location and size in structures using wavelet finite element methods". *Journal of Sound and Vibration,* **285**, p. 767–782 .

[8] Swamidas, A., Yang, X., and Seshadri, R., 2004. "Identification of cracking in beam structures using Timoshenko and Euler formulations". *Journal of Engineering Mechanics,* **130(11)**, pp. 1297–1308.

[9] Sinou, J.-J., 2007. "Numerical investigations of a robust identification of crack location and size in beams using only changes in ratio pulsations of the cracked beams". *Structural Engineering Mechanics,* **25(6)**, pp. 691–716.

[10] Owolabi, G., Swamidas, A., and Seshadri, R., 2003. "Crack detection in beams using changes in frequencies and amplitudes of frequency response functions". *Journal of Sound and Vibration,* **265**, pp. 1–22.

[11] Dilena, M., and Morassi, A., 2004. "The use of antiresonances for crack detection in beams". *Journal of Sound and Vibration,* **276**, p. 195–214 .

[12] Dilena, M., and Morassi, A., 2006. "Damage detection in discrete vibrating systems". *Journal of Sound and Vibration,* **289**, p. 830–850 .

[13] Dilena, M., and Morassi, A., 2002. "Identification of crack location in vibrating beams from changes in node positions". *Journal of Sound and Vibration,* **255(5)**, pp. 915–930 .

[14] Lele, S., and Maiti, S., 2002. "Modeling of transverse vibration of short beams for crack detection and measurement of crack extension". *Journal of Sound and Vibration,* **257 (3)**, p. 559–583 .

[15] Cerri, M. N., and Vestroni, F., 2000. "Detection of damage in beams subjected to diffused cracking". *Journal of Sound and Vibration,* **234(2)**, pp. 259–276.

[16] Sinou, J.-J., 2007. "Damage assessment based on the frequencies' ratio surfaces intersection method for the identification of the crack depth, location and orientation". *Structural Durability and Health Monitoring,* **3(3)**, pp. 134–162.

[17] Mottershead, J., and Friswell, M., 1993. "Model updating in structural dynamics: a survey". *Journal of Sound and Vibration,* **167 (2)**, pp. 347–375.

[18] Baruch, M., 1982. "Optimal correction of mass and stiffness matrices using measured modes". *AIAA Journal,* **20 (11)**, pp. 1623–1626.

[19] Berman, A., and Nagy, E., 1983. "Improvement of a large analytical model using test data". *AIAA Journal,* **21 (8)**, pp. 1168–1173.

[20] Berger, H., Ohayon, R., Quetin, L., Barthe, L., Ladevèze, P., and Reynier, M., 1991. *Updating methods for structural dynamics models : 9-20.* La Recherche Aérospatiale 5 (in French).

[21] Farhat, C., and Hemez, F., 1993. "Updating finite element dynamics models using an element-by-element sensitivity methodology". *AIAA Journal,* **31 (9)**, pp. 1702–1711.

[22] Piranda, J., Lallement, G., and Cogan, S., 1991. "Parametric correction of finite element modes by minimization of an output residual: improvement of the sensitivity method". *Proc. of the 9th International Modal Analysis Conference*.

[23] Lammens, S., Brughmans, M., Leuridan, J., Heylen, W., and Sas, P., 1995. "Application of a frf based model updating technique for the validation of a finite element model of components of the automotive industry". *ASME Conference,* **Boston**, pp. 1191–1200.

[24] Ladevèze, P., and Reynier, M., 1989. "Fe modeling and analysis: a localization method of stiffness errors and adjustments of fe models". *Vibrations Analysis Techniques and Application, ASME Publishers*.

[25] Ladevèze, P., Nedjar, D., and Reynier, M., 1994. "Updating of finite element models using vibrations tests". *AIAA Journal,* **32 (7)**, pp. 1485–1491.

[26] Ladevèze, P., and Chouaki, A., 1999. "Application of a posteriori error estimation for structural model updating". *Inverse Problems,* **15**, pp. 49–58.

[27] Chouaki, A., Ladevèze, P., and Proslier, L., 1998. "Updating structural dynamics models with emphasis on the damping properties". *AIAA Journal,* **36 (6)**, pp. 1094–1099.

[28] Balmès, E., 2000. "Review and evaluation of shape expansion methods". *Proc. of the 18th International Modal Analysis Conference*.

[29] Pascual, R., Golinval, J., and Razeto, M., 1998. "On the reliability of error localization indicators". *Proc. of the 23rd International Conference on Noise and Vibration Engineering (ISMA)*.

[30] Moine, P., Billet, L., and Aubry, D., 1995. "Updating a non conservative finite element model: two modal methods". *Proc. of the 3rd Design Engineering Technical Conference*.

[31] Bonnet, M., and Constantinescu, A., 2005. "Inverse problems in elasticity". *Inverse Problems,* **21(2)**, pp. 1–50.

[32] Dimarogonas, A., 1996. "Vibration of cracked structures: a state of the art review". *Applied Mechanics Review,* **55**, pp. 831–857 .

[33] Wauer, J., 1990. "Dynamics of cracked rotors: Literature survey". *Applied Mechanics Review,* **43**, pp. 13–17 .

[34] Davies, W. G. R., and Mayes, I. W., 1984. "The vibrational behaviour of a multi-shaft, multi-bearing system in the presence of a propagating transverse crack". *Transactions of the ASME Journal of Vibration, Acoustics, Stress, and Reliability in Design,* **106**, pp. 146–153.

[35] Mayes, I. W., and Davies, W. G. R., 1984. "Analysis of the response of a multi-rotor-bearing system containing a transverse crack in a rotor". *Transactions of the ASME Journal of Vibration, Acoustics, Stress, and Reliability in Design,* **106**, pp. 139–145.

[36] Mayes, I. W., and Davies, W. G. R., 1976. "The vibrational behaviour of a rotating shaft system containing a transverse crack". *IMechE Conference on Vibrations in Rotating Machinery, Cambridge, United Kingdom,* **1**, pp. 53–64.

[37] Sinou, J.-J., and Lees, A. W., 2005. "Influence of cracks in rotating shafts". *Journal of Sound and Vibration,* **285(4-5)**, pp. 1015–1037.

[38] Sinou, J.-J., and Lees, A. W., 2007. "A non-linear study of a cracked rotor". *European Journal of Mechanics - A/Solids,* **26(1)**, pp. 152–170.

[39] Ladevèze, P., 1998. "A modelling error estimator for dynamic structural model updating". *New Advances in Adaptive Computational Methods in Mechanics. Ed. P. Ladeveze and J.T. Oden,* pp. 135–51.

[40] Ladevèze, P., and Pelle, J.-P., 2005. *Mastering calculations in linear and nonlinear mechanics*. Springer.

[41] Deraemaeker, A., Ladevèze, P., and Romeuf, T., 2004. "Model validation in the presence of uncertain experimental data". *Engineering Computational,* **21 (8)**, pp. 808–833.

[42] Deraemaeker, A., Ladevèze, P., and Leconte, P., 2002. "Reduced based for model updating in structural dynamics based on constitutive relation error". *Computational Methods in Applied Mechanics and Engineering*, **191**, pp. 2427–2444.

[43] Liang, R., Choy, F., and Hu, J., 1991. "Detection of cracks in beam structures using measurements of natural frequencies". *Journal of the Franklin Institute*, **328(4)**, pp. 505–518.

[44] Adams, R., Cawley, P., Pye, C., and Stone, B., 1978. "A vibration technique for non-destructively assessing the integrity of structures". *Journal of Mechanical Engineering Science*, **20**, pp. 93–100.

[45] Morassi, A., 1993. "Crack-induced changes in eigenparameters of beam structures". *American Society of Civil Engineers, Journal of Engineering Mechanics*, **119**, pp. 1798–1803.

[46] Hearn, G., and Test, R., 1991. "Modal analysis for damage detection in structures". *American Society of Civil Engineers, Journal of Structural Engineering*, **117**, pp. 3042–3063.